Journal of Materials Chemistry A

PAPER

View Article Online
View Journal | View Issue

Cite this: J. Mater. Chem. A, 2014, 2, 20147

Design and synthesis of functional ionic liquids based on pyrrolidinium cations bearing alkyl nitrile moieties†

Shan Cong,[a] Yun Wang,[a] Qinghua Yi,[a] Jie Zhao,*[a] Yinghui Sun,[a] Mingrong Shen[b] and Guifu Zou*[a]

Received 1st September 2014
Accepted 9th October 2014

DOI: 10.1039/c4ta04523h

www.rsc.org/MaterialsA

A series of functional ionic liquids based on pyrrolidinium cations bearing alkyl nitrile moieties have been designed, synthesized and characterised with high purity and yield. The influence of the anion structure and methylene chain length of the alkyl nitrile moieties on the thermal properties of functional ionic liquids is comprehensively investigated. Moreover, some of the ionic liquids show obvious plastic crystal phase behavior with rotational disorder and activated vacancies/defects, which can offer a solid bulk matrix for doping 1-propyl-3-methylimidazolium iodine (PMII), LiI and I_2 to prepare plastic crystal electrolytes with high melting points and conductivities. Furthermore, the resulting solid-state dye-sensitized solar cell (DSSC) exhibits a power conversion efficiency (PCE) of 5.22% under the simulated air mass 1.5 solar spectrum illumination at 100 mW cm^{-2}, and displays a superior long-term stability compared to conventional liquid-based devices. These results offer us a feasible method to explore new organic plastic crystals and electrolytes for high temperature solid-state DSSCs.

Introduction

Ionic liquids (ILs) are mostly liquid organic salts with melting points below/near room temperature.[1] During the last two decades, due to their negligible vapor pressure, high chemical and thermal stability and unique ionic environment, ionic liquids have been widely used as green and sustainable solvents in synthesis, catalysis and petrochemical industries.[2,3] In addition, high ionic conductivities, large viscosity range and wide electrochemical windows also render them to be a promising source for liquid or solid electrolytes for renewable energy devices, such as lithium batteries and dye-sensitized solar cells.[4,5]

Recently, functional ionic liquids, with rationally designed structural groups, have attracted great attention for an extended research interest. For example, the rigidity and cubic structure of the polyhedral oligomeric silsesquioxane (POSS) moiety can enhance the thermal stability and significantly reduce the melting temperature of POSS ionic liquids.[6] By employing propylene carbonate, several polycarbonate (PC) functional ionic liquids are rationally designed with a wide thermal stability, which exhibit a potential ability for lithium metal deposition.[7] Ferrocene-based ionic liquids also represent excellent electroactive and fine charge transport properties, which extend the chemical diversity of intrinsically redox ionic liquid phases.[8] By virtue of the amine fixation function to form an ammonium carbamate, task-specific ionic liquids prove the notable sequestration efficiency of CO_2.[9] Due to the formation of surface protective groups with a lubricated metal surface *via* a tribochemical reaction and good miscibility of ILs with polyurea grease, ILs also show a potential use as additives for the rolling bearings industry.[10] A variety of task specific ionic liquids (TSIL) can be used to prepare N-doped microporous and mesoporous carbons with a high surface area of over 640 m^2 g^{-1}, thus highlighting exciting opportunities in functional carbon composites.[11] Full color-tunable luminescent emissions can be successfully achieved by simply tuning or changing the moieties of ionic liquid crystals, thus displaying potential applications in fluorescent sensors and optoelectronic materials.[12] Therefore, functional ionic liquids offer an opportunity to demonstrate their basic research interest and extensive promising applications.

Here, we design and synthesize a series of functional ionic liquids containing pyrrolidinium cations bearing alkyl nitrile moieties and anions (I^-, PF_6^- and $TFSI^-$). Their chemical structures and thermal properties are confirmed and characterized in detail by Fourier transform infrared (FTIR) spectra, nuclear magnetic resonance (NMR) measurement, thermogravimetric (TGA) and differential scanning calorimetry (DSC) analysis. These ionic liquids exhibit different thermal

[a]College of Physics, Optoelectronics and Energy & Collaborative, Innovation Center of Suzhou Nano Science and Technology, Soochow University, Suzhou 215006, P. R. China. E-mail: jzhao@suda.edu.cn; zouguifu@suda.edu.cn; Fax: +86-512-65228130; Tel: +86-512-65228130

[b]Jiangsu Key Lab of Thin Films, Soochow University, P. R. China

† Electronic supplementary information (ESI) available: Additional tables (PDF). See DOI: 10.1039/c4ta04523h

properties, which are beneficial to understand the alkyl nitrile and anions structure effect. Notably, some of the synthesized ionic liquids represent obvious plastic crystal phases, which lead to high intrinsic ionic conductivity. As an application, doping the ionic liquid 1-propyl-3-methylimidazolium iodide (PMII) and LiI can still retain the plastic crystal behaviors, and further enhance the ionic conductivity of the prepared high temperature solid state electrolytes without any volatile organic solvent for their application in dye-sensitized solar cells (DSSCs). The fabricated DSSC shows a high power conversion efficiency over 5% and displays better long-term stability than that of referenced organic liquid electrolytes.

Experimental procedure

Materials

Iodomethane, 1-pyrroleacetonitrile, 1-pyrrolidinepropanenitrile, 1-pyrrolidinobutyronitrile, lithium iodide (LiI), 4-*tert*-butylpyridine (TBP), 3-methoxypropionitrile (MPN) and iodine (I_2) were purchased from Alfa Aesar and used as received. Potassium hexafluorophosphate (KPF_6), lithium bis(trifluoromethanesulfonyl)imide (LiTFSI), 1-propyl-3-methylimidazolium iodine (PMII) and 1,2-dimethyl-3-propylimidazolium iodide (DMPII) were purchased from Merck. H_2PtCl_6 and the organic dye 2-cyano-3-[5‴-(9-ethyl-9*H*-carbazol-3-yl)-3′,3″,3‴4-tetra-*n*-hexyl-[2,2′,5′,2″,5″,2‴]-quaterthiophenyl-5-yl]acrylic acid (MK-2) were purchased from Aldrich. All the chemical reagents were used without further treatment. Fluorine-doped tin oxide (FTO) glass electrodes (8 Ω Sq^{-1}) and slurries containing 20 nm-sized mesoporous and 200 nm-diameter light-scattering TiO_2 colloids were purchased from Dalian Hepat Chroma Solar Tech. Co., Ltd (China).

General synthetic procedure of 1-cyanomethyl-1-methylpyrrolidinium iodide (CMMPI), 1-cyanomethyl-1-methylpyrrolidinium hexafluorophosphate ($CMMPPF_6$) and 1-cyanomethyl-1-methylpyrrolidinium bis(trifluoromethanesulfonyl)imide (CMMPTFSI)

CMMPI was synthesized as follows: briefly, a mixture of iodomethane (20 mmol, 2.84 g) and 1-pyrrolidineacetonitrile (20 mmol, 2.2 g) in 20 mL ethanol was stirred at 60 °C for 12 h under an atmosphere of nitrogen. After the evaporation of solvent, the crude product was washed with diethyl ether three times and dried under vacuum at 60 °C for 24 h to obtain 4.59 g CMMPI (yield: 91%, brown powder). mp: 30.2 °C; ^{1}HNMR: (400 MHz, d_6-DMSO): 4.90 (s, 2H), 3.64–3.70 (m, 2H), 3.55–3.62 (m, 2H), 3.20 (s, 3H), 2.10–2.16 (m, 4H) (see ESI, Fig. S1†).

The anion exchange of CMMPI with KPF_6 in aqueous solution yielded $CMMPPF_6$ (yield: 86%, brown powder). mp, 22.6 °C; ^{1}HNMR: (400 MHz, d_6-DMSO): 3.69–3.75 (t, 2H), 3.42–3.58 (m, 4H), 3.17–3.24 (t, 3H), 3.02–3.07 (s, 3H), 2.05–2.15 (m, 4H) (see ESI, Fig. S1†).

Moreover, CMMPTFSI was synthesized by the anion exchange of CMMPI with LiTFSI (yield: 85%, white powder). ^{1}HNMR: (400 MHz, d_6-DMSO): 4.86–4.90 (s, 2H), 3.64–3.72 (m, 2H), 3.20–3.24 (s, 3H), 2.12–2.20 (m, 4H) (see ESI, Fig. S1†).

Synthesis of 1-cyanoethyl-1-methylpyrrolidinium iodide (CEMPI), 1-cyanoethyl-1-methylpyrrolidinium hexafluorophosphate ($CEMPPF_6$) and 1-cyanoethyl-1-methylpyrrolidinium bis(trifluoromethanesulfonyl)imide (CEMPTFSI)

The same procedure was followed as described above, except for the use of 1-pyrrolidinepropionitrile (2.48 g, 20 mmol) instead of 1-pyrrolidineacetonitrile. CEMPI (yield: 88%, brown powder); mp: 126 °C; ^{1}HNMR: (400 MHz, d_6-DMSO): 3.69–3.74 (t, 2H), 3.50–3.56 (m, 2H), 3.44–3.50 (m, 2H), 3.18–3.22 (t, 2H), 3.03 (s, 3H), 2.05–2.11 (m, 4H) (see ESI, Fig. S2†). $CEMPPF_6$ (yield: 84%, brown powder); mp, 78 °C; ^{1}HNMR: (400 MHz, d_6-DMSO): 3.68–3.75 (t, 2H), 3.44–3.58 (m, 4H), 3.17–3.24 (m, 2H), 3.03 (s, 3H), 2.04–2.16 (m, 4H) (see ESI, Fig. S2†). CEMPTFSI (yield: 84%, brown powder); ^{1}HNMR: (400 MHz, d_6-DMSO): 3.69–3.75 (t, 2H), 3.42–3.58 (m, 4H), 3.17–3.24 (m, 2H), 3.04 (s, 3H), 2.06–2.14 (m, 4H) (see ESI, Fig. S2†).

Synthesis of 1-cyanopropyl-1-methylpyrrolidinium iodide (CPMPI), 1-cyanopropyl-1-methylpyrrolidinium hexafluorophosphate ($CPMPPF_6$) and 1-cyanopropyl-1-methylpyrrolidinium bis(trifluoromethanesulfonyl)imide (CEMPTFSI)

The same procedure was followed as described above, except for the use of 1-pyrrolidinobutyronitrile (2.74 g, 20 mmol) instead of 1-pyrrolidinepropionitrile. CPMPI (yield: 88%, brown powder); mp: 141 °C; ^{1}HNMR: (400 MHz, d_6-DMSO): 3.44–3.57 (m, 4H), 3.36–3.42 (m, 2H), 3.02 (s, 3H), 2.61–2.67 (m, 2H), 2.03–2.13 (m, 6H) (see ESI, Fig. S3†). $CPMPPF_6$ (yield: 84%, brown powder); mp, 226 °C; ^{1}HNMR: (400 MHz, d_6-DMSO): 3.40–3.56 (m, 4H), 3.35–3.40 (m, 2H), 3.0 (s, 3H), 2.58–2.65 (m, 2H), 2.02–2.15 (m, 6H) (see ESI, Fig. S3†). CPMPTFSI (yield: 84%, brown powder); ^{1}HNMR: (400 MHz, d_6-DMSO): 3.40–3.56 (m, 4H), 3.35–3.40 (m, 2H), 3.0 (s, 3H), 2.58–2.66 (m, 2H), 2.03–2.15 (m, 6H) (see ESI, Fig. S3†).

Device fabrication

The DSSCs were assembled as documented in the previous literature.[13] The cleaned FTO glass was covered at two parallel edges with an adhesive tape to control the thickness of the mesoporous TiO_2 film. Two layers of TiO_2 particles were deposited onto the cleaned FTO glass and used as photoelectrodes. A 10 μm thick film of 20 nm-sized TiO_2 particles was deposited onto the FTO glass electrode by the doctor-blade technique. The film was dried at 125 °C for 5 min. Then, a second 5 μm thick layer of 200 nm light-scattering anatase particles were coated on the top of the first TiO_2 layer. The resulting TiO_2 films were annealed at 500 °C for 15 min. After cooling to 80 °C, the obtained TiO_2 electrode was immersed in 0.3 mM solution of MK-2 in anhydrous toluene at room temperature for 12 h. The dyed TiO_2 electrode was washed with anhydrous ethanol and dried under a nitrogen stream. To prepare the Pt counter electrode, two drops of 5 mM H_2PtCl_6 in ethanol was placed onto the cleaned FTO glass substrate, followed by drying and annealing at 400 °C for 15 min.

The electrolytes A–G, composed of 0–40 wt% PMII and CPMPI with/without 0.1 M LiI and 0.10 M I_2, were heated at 120 °C and stirred for 8 h to ensure homogeneity. After cooling down to room temperature, all the solid-state electrolytes were formed.

DSSCs were fabricated by sandwiching the methanol solution of electrolyte G between a dye-sensitized TiO_2 electrode and a pre-drilled Pt counter electrode by a 40 μm hot melt ring (Surlyn, DuPont). The resulting cells were placed in vacuum to remove air to guarantee optimum filling and fine electrical contact. The produced devices were sealed with a Surlyn sheet and a thin glass cover by heating.

Characterization and measurements

^{1}HNMR spectra were recorded on a Varian 400 MHz spectrometer. Fourier transform infrared (FTIR) spectra of the synthesized compounds were recorded on a Varian CP-3800 spectrometer in the range of 4000–400 cm^{-1}. Thermal analysis was carried out on Universal Analysis 2000 thermogravimetric analyzer (TGA). Samples were heated from 50 to 500 °C at a heating rate of 10 °C min^{-1} under a nitrogen flow. Differential scanning calorimetry (DSC) measurements were performed under a nitrogen atmosphere with a heating rate of 10 °C min^{-1} in a temperature range of −50–300 °C on a DSC-Q200. The conductivity of the electrolytes was characterized in a cell composed of a Teflon tube and two identical stainless steel electrodes on a CHI660c electrochemical workstation, using the AC impedance method over the frequency range of 1–10^5 Hz. All the samples were equilibrated for at least 20 min at a given temperature. The photocurrent density–voltage (J–V) curves of the assembled DSSCs shielded by an aluminum foil mask with an aperture area of ≈0.25 cm^2 were measured with a digital source meter (Keithley, model 2400) under simulated air mass (AM) 1.5 solar spectrum illumination at 100 mW cm^{-2}. The incident photo-to-current conversion efficiency (IPCE) plotted as a function of excitation wavelength was recorded under the irradiation of a xenon lamp with a monochromater (Oriel CornerstoneTM 260 1/4). The photoelectrochemical parameters, such as the fill factor (FF) and power conversion efficiency (PCE), were calculated according to the previous reports.[13]

Results and discussion

Scheme 1 shows the synthetic route and chemical structures of the functional ionic liquids containing pyrrolidinium cations with different alkyl nitrile moieties and anions. The purity and chemical structure are confirmed by ^{1}HNMR (Fig. S1–S3, ESI†) and FTIR spectra. Moreover, Fig. 1 exhibits the typical images of CEMPI, $CEMPPF_6$ and CEMPTFSI. In addition, all the images of the synthesized compounds in this work can be found in Fig. S4.† Obviously, compared with other compounds with anions of I^- and PF_6^-, CMMPTFSI, CEMPTFSI and CPMPTFSI display a liquid state behavior, probably because of weaker van der Waals forces.[14]

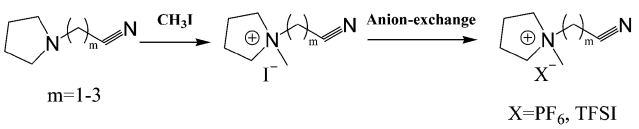

Scheme 1 Synthetic procedures for the preparation of a series of functional ionic liquids containing pyrrolidinium cations bearing alkyl nitrile moieties.

As shown in Fig. 2, typically, the chemical structures of CPMPI, $CPMPPF_6$ and CPMPTFSI are confirmed by FTIR spectra. The bands attributed to the pyrrolidinium cations between 3300 and 3650 cm^{-1} are clearly identified. Moreover, the adsorption peaks centred at 2900–3000 cm^{-1} and 1464 cm^{-1} are attributed to the C–H stretching vibration mode of the methylene chain and the alkyl chains. In all the FTIR spectra, the characteristic peaks of the C≡N stretching vibrations at 2245 cm^{-1} are observed. In addition, the anion exchange could be identified by the appearance of new bands. Compared with the absorption peak of anion I^- of CPMPI at 906 and 750 cm^{-1} in Fig. 1a, new bands corresponding to the PF_6^- anion in Fig. 1b are observed at 841 and 560 cm^{-1}.[15] The characteristic absorption peaks at 1348, 1202 and 1055 cm^{-1} belonging to TFSI anion in Fig. 1c, are also highly intensified,[15,16] indicating the successful anion exchange.

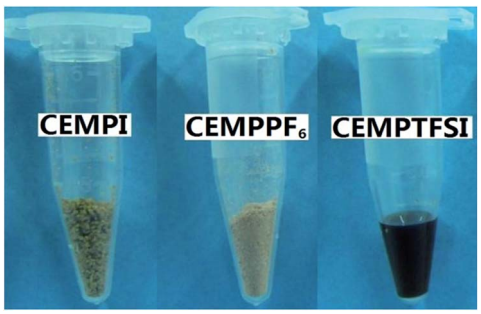

Fig. 1 Typical images of the synthesized CEMPI, $CEMPPF_6$ and CEMPTFSI.

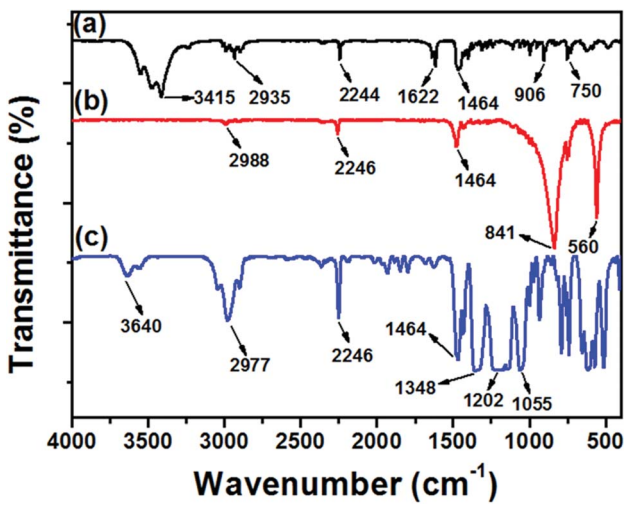

Fig. 2 FTIR spectra of (a) CPMPI, (b) $CPMPPF_6$ and (c) CPMPTFSI.

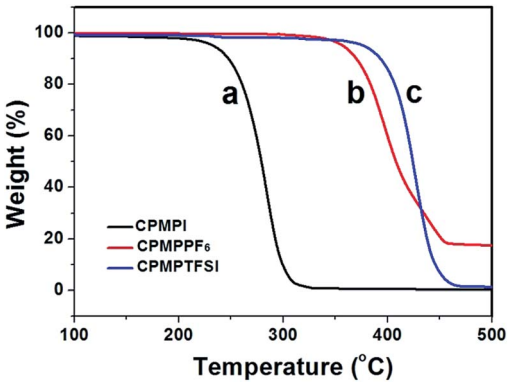

Fig. 3 TGA curves of (a) CPMPI, (b) $CPMPPF_6$ and (c) CPMPTFSI.

Moreover, all the FTIR spectra of the synthesized ionic liquids are shown in Fig. S5,† which reveal similar results of anion exchange.

The influence of the counteranions on the thermal stability of the produced functional ionic liquids was also studied. Fig. 3 shows the typical TGA curves of CPMPI, $CPMPPF_6$ and CPMPTFSI. The initial decomposition temperature of CPMPI is about 258 °C (Fig. 3a), indicating its high thermal stability. However, the anion exchange of CPMPI with PF_6^- and $TFSI^-$ presents much better thermostability, with corresponding values of 365 and 405 °C, respectively. The influence of the anion structure on the thermal stability is in the order of I^- < PF_6^- < $TFSI^-$, in agreement with the previously observed trends.[15] Moreover, the TGA curves of other ionic liquids with different alkyl nitrile moieties and anions are shown in Fig. S6.† The thermal properties of the ionic liquids are summarized in Table 1 as well. The corresponding decomposition temperature values of CMMPI, $CMMPPF_6$ and CMMPTFSI are 204, 305 and 340 °C. However, CEMPI, $CEMPPF_6$ and CEMPTFSI with a methylene chain length of 2C represent considerably lower initial decomposition temperature (180, 212 and 202 °C), as in previous reports,[17] probably due to the strong interaction of the nitrile groups with the pyrrolidinium rings. This result is also supported with the subsequent DSC analysis.

Table 1 TGA and DSC results for functional ionic liquids

	TGA	DSC			
	T_{onset}[a]	Mp[b]	T_d[c]	$T_{S-S\ I}$[d]	$T_{S-S\ II}$[e]
CMMPI	204	30.2	209	14.1	—
$CMMPPF_6$	305	22.6	281	—	—
CMMPTFSI	340	—	—	—	—
CEMPI	180	126	187	—	—
$CEMPPF_6$	212	78	—	60	—
CEMPTFSI	202	—	—	—	—
CPMPI	258	141	285	121	95
$CPMPPF_6$	365	226	—	95	—
CPMPTFSI	405	—	—	—	—

[a] Initial decomposition temperature by TGA. [b] Melting point. [c] Decomposition temperature by DSC on heating. [d] Temperature of solid–solid transition I. [e] Temperature of solid–solid transition II. [—] no measurement.

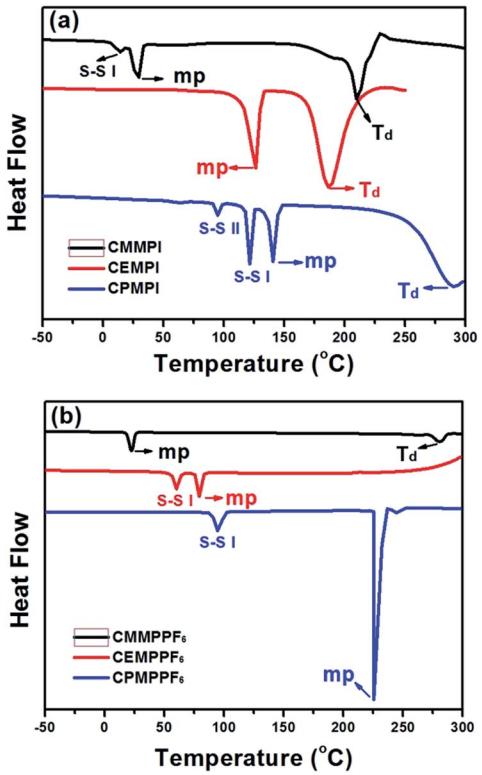

Fig. 4 The DSC curves of (a) CMMPI, CEMPI and CPMPI; (b) $CMMPPF_6$, $CEMPPF_6$ and $CPMPPF_6$.

Further investigation on the thermal stability by differential scanning calorimetry (DSC) is shown in Fig. 4. The thermal properties of the ionic liquids are also summarized in Table 1. Obviously, the melting points generally increase with increasing methylene chain length from 1 C to 3 C because of high symmetry and low rotational degrees of freedom determined by enhanced van der Waals interactions.[18,19] In Fig. 4a, the melting points of CMMPI, CEMPI and CPMPI are 30.2, 126 and 141 °C, respectively, whereas their decomposition temperatures (T_d) are 209, 187 and 285 °C. It should be noted that a methylene chain length with 2C significantly decreases the thermal stability of CEMPI, in accordance with the TGA results. As shown in Fig. 4b, the values of melting points increase in the order of $CMMPPF_6$ < $CEMPPF_6$ < $CPMPPF_6$, corresponding to 30.2, 126 and 141 °C, respectively. More interestingly, CMMPI, CPMPI, $CEMPPF_6$ and $CPMPPF_6$ exhibit one or two solid–solid phase transitions (S–S I and S–S II). The $T_{S-S\ I}$ values are 14.1, 60, 121 and 95 °C, respectively, suggesting a wide plastic phase range. However, CPMPI also shows a solid–solid phase transition temperature at 95 °C, indicating another form of molecular rotamer. This unique phenomenon donates some ionic crystals as organic plastic crystals, which have been extensively investigated by MacFarlane's and other research groups.[18–24]

Organic plastic crystals are a type of compound composed of organic molecules, which are rotationally disordered.[25] The existence of one or several solid–solid phase transitions below

the melting point endows organic plastic crystals with not only plastic properties and good mechanical flexibility, but also favorable rotational disorder and activated vacancies/defects, resulting in an effective migration of ions (Li^+, H^+, and I^-) and high ionic conductivity. Therefore, solid state electrolytes based on organic plastic crystals have been widely used for lithium ion cells[20,26] and dye-sensitized solar cells,[27,28] thus they can present great potential application in electrochemical devices.

The impressive plastic behaviors by the synthesized compounds and the abovementioned discussion triggered our interest in further exploring the possibility to fabricate a solid state DSSCs based on nitrile-functional plastic crystals. The relatively high melting point (141 °C) and solid–solid phase change temperatures (95 and 121 °C) render CPMPI to be one of the high temperature solid state electrolytes, which can overcome the leakage, evaporation and high temperature instability of conventional organic liquid electrolytes under practical outdoor conditions over 60–80 °C.[29] Therefore, as shown in Fig. 5, different weight ratios of PMII doped CPMPI based solid state electrolytes were prepared and characterized by DSC. Obviously, the sequential addition of 10–40 wt% PMII significantly decreases the melting point of CPMPI. However, the solid–solid phase transition temperature ($T_{S-S\ I}$) decreases only from 121 to 107 °C, demonstrating that PMII doped CPMPI based solid state electrolytes still retained its solid state property and plastic behavior. These results also indicate that PMII can be successfully incorporated into the bulk matrix of CPMPI to form a solid solution, which can act to be an effective ionic migration species for solid state electrolytes. It should be noted that 40 wt% PMII doped CPMPI plastic crystal electrolyte is completely solid at 100 °C, far beyond the outdoor operating requirement for solid state DSSCs.

It has been demonstrated that high ionic conductivity is critical for the performance of solid state DSSCs. Table 2 summarizes the conductivity for 0–40 wt% PMII doped CPMPI plastic crystal electrolytes with different I_2 and LiI contents (electrolyte A–G). It can be clearly seen that the conductivity of all the solid state electrolytes increases with the PMII content. Compared with the pure CPMPI (4.23×10^{-5} S cm^{-1}) and other weight ratios of PMII doped electrolyte A–D, the 40 wt% PMII doped CPMPI electrolyte E shows the highest conductivity with the value of 1.01×10^{-4} S cm^{-1}, probably due to the high bulk conductivity of PMII (6.0×10^{-4} S cm^{-1}) and decoupling of rational disorder and the existence of vacancies and defects in the lattice of the plastic crystal (CPMPI in this work).[21] Notably, further doping I_2 into electrolyte E can significantly enhance the conductivity of the prepared electrolyte F and G, respectively. This increase in ionic conductivity originates from the formation of polyiodides by the reaction of I^- and I_2 species,[30] accelerating the charge transport along the polyiodides chain by the Grotthuss-type electron-exchange mechanism. The mechanism can also be expressed by the Dahm–Ruff equation (eqn (1)) as follows:[31]

$$D_{app} = 1/6k_{ex}\delta^2 c + D_{phys} \quad (1)$$

where D_{app} is the apparent diffusion coefficient of I^- and I_3^-, D_{phys} is physical diffusion, k_{ex} is the rate constant of electron exchange, and c and δ are the concentration and average center-to-center distances between the redox species, respectively. Thus, the high conductivity of 3.74×10^{-4} S cm^{-1} for electrolyte F is successfully obtained. In addition, LiI can be further incorporated into the matrix of electrolyte F to form electrolyte G, resulting in the higher conductivity of 4.26×10^{-4} S cm^{-1}. The increased bulk concentration of iodide and Li^+ ions,[32] creation of vacancies and defects in the lattice of CPMPI as an additional charge carrier,[33] and the interaction between Li^+ and nitrile groups[34] facilitates the charge transfer of I^- along the polyiodides chain, which should be responsible for the enhancement in the conductivity of electrolyte G. For these reasons, electrolyte G is thus selected for the fabrication of solid–state DSSC in this work.

Table 2 The components and conductivity of the electrolytes at room temperature in this work

Electrolyte	PMII[a] [wt%]	Conductivity [10^{-5} S cm^{-1}]	I_2 [M]	LiI [M]
Electrolyte A	0	4.23	—	—
Electrolyte B	10	6.15	—	—
Electrolyte C	20	7.73	—	—
Electrolyte D	30	9.08	—	—
Electrolyte E	40	10.12	—	—
Electrolyte F	40	37.43	0.1	—
Electrolyte G	40	42.58	0.1	0.1

[a] Weight ratios of PMII/CPMPI varies from 0 to 40 wt%.

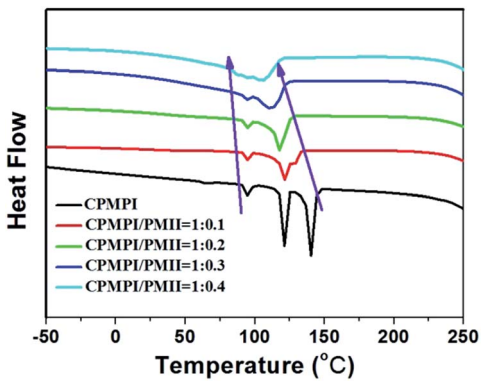

Fig. 5 DSC curves of CPMPI, and PMII doped CPMPI with different weight ratios.

The photocurrent density–voltage (J–V) curve of the fabricated device based on electrolyte G is shown in Fig. 6a. The values of the open-circuit voltage (V_{oc}), short-circuit current density (J_{sc}), and fill factor (FF) are 0.675 V, 10.32 mA cm^{-2} and 0.749, respectively, yielding a power conversion efficiency (PCE) of 5.22%. Moreover, as shown in Fig. 6b, the incident photon-to-current conversion efficiency (IPCE) exceeds 50% in a broad spectral range from 400 to 650 nm and reaches the maximum value of about 67.5% at 510 nm, indicating high light harvesting efficiency, fast electron injection, and effective dye regeneration

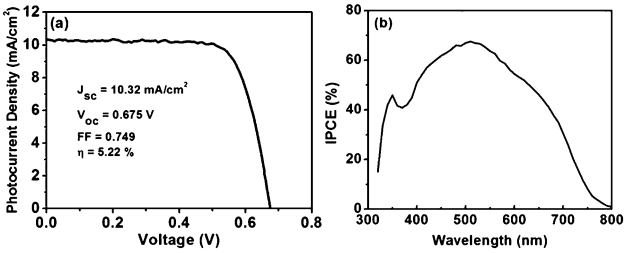

Fig. 6 (a) Photocurrent density–voltage (J–V) curve and (b) IPCE *vs.* wavelength profiles for the high temperature solid-state DSSC based on electrolyte G. Cell area: 0.25 cm^2.

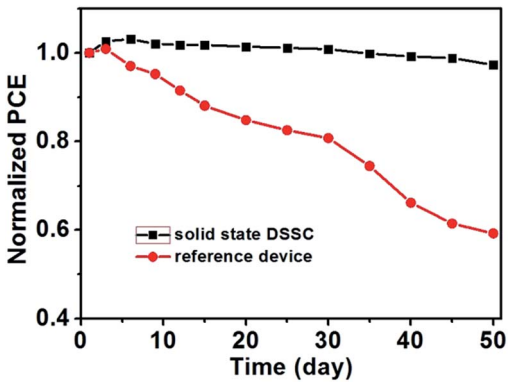

Fig. 7 Time-course variation of normalized PCE for the fabricated solid-state DSSC and reference device with successive one sun light soaking during the accelerated aging test at 60 °C. A typical organic liquid electrolyte for the reference device contains 0.6 M DMPII, 0.1 M LiI, 0.5 M TBP, 0.1 M I_2 in MPN.[13]

and charge collection for the high temperature solid-state DSSC.

The long-term stabilities of the abovementioned solid-state DSSC and reference device containing an organic liquid electrolyte at 60 °C under the same conditions were also investigated and are presented in Fig. 7. During the first three days, the efficiency was moderately enhanced along with an increase of J_{sc} originating from the regeneration of MK-2 dye and improvement of the interfacial contact between TiO_2 and the plastic crystal electrolyte.[35,36] More importantly, due to the high temperature solid property of the employed plastic electrolyte, the solid-state DSSC still retained almost over 97% of its initial conversion efficiency after the aging test of 50 days, indicating excellent stability. For comparison, the reference device fabricated with an organic liquid electrolyte maintains only about 60% of its initial conversion efficiency. These results of the stability tests demonstrate that the fabricated solid-state DSSC could overcome the leakage and evaporation of organic components in conventional DSSCs.

Conclusions

In summary, a series of functional ionic liquids based on pyrrolidinium cations bearing alkyl nitrile moieties have been designed, synthesized and characterized. They were successfully prepared with high purity and yield. With respect to the anion structure, the thermal stability is in the order of $I^- < PF_6^- < TFSI^-$. Moreover, increasing the methylene chain length from 1 C to 3 C of pyrrolidinium cations bearing alkyl nitrile moieties can increase the melting points of the solid ionic crystals. Moreover, some of the ionic liquids show obvious plastic crystal phase behavior with rotational disorder and activated vacancies/defects, which can offer a solid bulk matrix for doping PMII, LiI an I_2 to prepare plastic crystal electrolytes with high conductivity. Furthermore, the fabricated high temperature solid-state DSSC exhibits a high efficiency of 5.22% and displays more excellent long-term stability than conventional liquid-based devices. These results offer us a feasible method to synthesize organic plastic crystals and electrolytes for high performance solid-state DSSCs for future practical applications.

Acknowledgements

This work was supported by "973 Program" Special Funds for the Chief Young Scientist (no. 2015CB358600), Postdoctoral Science Foundation Grant of China (no. 2013M531397), University Science Research Project of Jiangsu Province (no. 13KJB150033), the Natural Science Foundation of Jiangsu Province (no. BK20140311), the Open Foundation of Jiangsu Key Laboratory of Thin Films and the Project Funded by the PAPD of Jiangsu Higher Education Institutions.

Notes and references

1 R. D. Rogers, K. R. Seddon and S. Volkov, in *Green Industrial Applications of Ionic Liquids; NATO Science. Series*, Kluwer, Boston, 2002.
2 T. Welton, *Chem. Rev.*, 1999, **99**, 2071–2083.
3 V. I. Pârvulescu and C. Hardacre, *Chem. Rev.*, 2007, **107**, 2615–2665.
4 M. Armand, K. Endres, D. R. MacFarlane, H. Ohno and B. Scrosati, *Nat. Mater.*, 2009, **8**, 621–629.
5 S. M. Zakeeruddin and M. Grätzel, *Adv. Funct. Mater.*, 2009, **19**, 2187–2202.
6 K. Tanaka, F. Ishiguro and Y. Chujo, *J. Am. Chem. Soc.*, 2010, **132**, 17649–17651.
7 T. Tsuda, K. Kondo, T. Tomioka, Y. Takahashi, H. Matsumoto, S. Kuwabata and C. L. Hussey, *Angew. Chem., Int. Ed.*, 2010, **50**, 1310–1313.
8 R. Balasubramanian, W. Wang and R. W. Murray, *J. Am. Chem. Soc.*, 2006, **128**, 9994–9995.
9 E. D. Bates, R. D. Mayton, I. Ntai and J. H. Davis Jr, *J. Am. Chem. Soc.*, 2002, **124**, 926–927.
10 M. Cai, Z. Zhao, Y. Liang, F. Zhou and W. Liu, *Tribol. Lett.*, 2010, **40**, 215–224.
11 J. S. Lee, Q. Wang, H. Luo, G. A. Baker and S. Dai, *J. Am. Chem. Soc.*, 2009, **131**, 4596–4597.
12 K. Tanabe, Y. Suzui, M. Hasegawa and T. Kato, *J. Am. Chem. Soc.*, 2012, **134**, 5652–5661.
13 J. Zhao, F. Yan, L. Qiu, Y. Zhang, C. Chen and B. Sun, *Chem. Commun.*, 2011, **47**, 11516–11518.

14 N. V. Plechkova and K. R. Seddon, *Chem. Soc. Rev.*, 2008, **37**, 123–134.
15 J. Zhao, F. Yan, Z. Chen, H. Diao, F. Chu, S. Yu and J. Lu, *J. Polym. Sci., Part A: Polym. Chem.*, 2009, **47**, 746–753.
16 X. Chen, J. Zhao, J. Zhang, L. Qiu, D. Xu, H. Zhang, X. Hang, B. Sun, G. Fu, Y. Zhang and F. Yan, *J. Mater. Chem.*, 2012, **22**, 18018–18024.
17 S. Schneider, T. Hawkins, Y. Ahmed, S. Deplazes and J. Mills, Ionic Liquid Fuels for Chemical Propulsion, in *Ionic Liquids: Science and Application*, ACS Symp. Ser., 2012, vol. 111, pp. 1–25.
18 S. J. Pas, J. M. Pringle, M. Forsyth and D. R. MacFarlane, *Phys. Chem. Chem. Phys.*, 2004, **6**, 3721–3725.
19 Z. Zhou, H. Matsumoto and K. Tatsumi, *ChemPhysChem*, 2005, **6**, 1324–1332.
20 D. R. MacFarlane, J. Huang and M. Forsyth, *Nature*, 1999, **402**, 792–794.
21 D. R. MacFarlane and M. Forsyth, *Adv. Mater.*, 2001, **13**, 957–966.
22 J. M. Pringle, P. C. Howlett, D. R. MacFarlane and M. Forsyth, *J. Mater. Chem.*, 2010, **20**, 2056–2062.
23 Y. Abu-Lebdeh, P. J. Alarco and M. Armand, *Angew. Chem., Int. Ed.*, 2003, **42**, 4499–4501.
24 Z. Zhou, H. Matsumoto and K. Tatsumi, *ChemPhysChem*, 2004, **10**, 6581–6591.
25 J. Adebahr, A. J. Seeber, D. R. MacFarlance and M. Forsyth, *J. Phys. Chem. B*, 2005, **109**, 20087–20092.
26 P. J. Alarco, Y. Abu-Lebdeh, A. Abouimrane and M. Armand, *Nat. Mater.*, 2004, **3**, 476–481.
27 V. Armel, M. Forsyth, D. R. MacFarlane and J. M. Pringle, *Energy Environ. Sci.*, 2011, **4**, 2234–2239.
28 Q. Li, J. Zhao, B. Sun, B. Lin, L. Qiu, Y. Zhang, X. Chen, J. Lu and F. Yan, *Adv. Mater.*, 2012, **24**, 945–950.
29 M. Grätzel, *J. Photochem. Photobiol., A*, 2004, **164**, 3–14.
30 J. H. Wu, S. C. Hao, Z. Lan, J. M. Lin, M. L. Huang, Y. F. Huang, P. J. Li, S. Yin and T. Sato, *J. Am. Chem. Soc.*, 2008, **130**, 11568–11569.
31 R. Kawano and M. Watanable, *Chem. Commun.*, 2005, 2107–2109.
32 Q. Li, X. Chen, J. Zhao, L. Qiu, Y. Zhang, B. Sun and F. Yan, *J. Mater. Chem.*, 2012, **22**, 6674–6679.
33 Y. Shekibi, J. M. Pringle, J. Sun, S. J. Pas, N. M. Rocher, B. R. Clare, A. J. Hill, D. R. Macfarlane and M. Forsyth, *J. Mater. Chem.*, 2010, **20**, 338–344.
34 H. X. Wang, B. F. Xue, Y. S. Hu, Z. X. Wang, Q. B. Meng, X. J. Huang and L. Q. Chen, *Electrochem. Solid-State Lett.*, 2004, **7**, A302–A305.
35 B. A. Gregg, F. Pichot, S. Ferrere and C. L. Fields, *J. Phys. Chem. B*, 2001, **105**, 1422–1429.
36 H. Wang, J. Li, F. Gao, G. Zhou and Z. Wang, *J. Am. Chem. Soc.*, 2013, **135**, 12627–12633.